Volume-Rendered Projection-Resolved OCT Angiography: 3D Lesion Complexity Is Associated With Therapy Response in Wet Age-Related Macular Degeneration

Peter L. Nesper,[1] Brian T. Soetikno,[1–3] Alison D. Treister,[1] and Amani A. Fawzi[1]

[1]Department of Ophthalmology, Feinberg School of Medicine, Northwestern University, Chicago, Illinois, United States
[2]Functional Optical Imaging Laboratory, Department of Biomedical Engineering, Northwestern University, Evanston, Illinois, United States
[3]Medical Scientist Training Program, Feinberg School of Medicine, Northwestern University, Chicago, Illinois, United States

PURPOSE. To explore whether quantitative three-dimensional (3D) analysis of choroidal neovascularization (CNV) using projection-resolved optical coherence tomography angiography (PR-OCTA) is associated with treatment response in neovascular age-related macular degeneration (nAMD).

METHODS. Retrospective, cross-sectional study of 51 eyes of 49 patients undergoing individualized anti-VEGF therapy for nAMD. Patients were classified as "good" or "poor" responders, requiring injections at less or more frequently than 6-week intervals, respectively. Cross-sectional PR-OCTA images were used to measure the distance between Bruch's membrane and highest CNV flow signal. The number of flow layers within the CNV and the distance between these flow layers (CNV flow thickness) were also analyzed. Two masked, independent graders measured the PR-OCTA parameters. We used 3D volume-rendered PR-OCTA to confirm the number of CNV flow layers and further evaluate CNV complexity.

RESULTS. Poor responders had significantly greater distance between Bruch's membrane and highest CNV flow signal ($P < 0.01$), greater number of CNV flow layers ($P = 0.022$), and greater CNV flow thickness ($P < 0.01$). Volume-rendered PR-OCTA images confirmed the number of CNV flow layers.

CONCLUSIONS. Cross-sectional and 3D volume-rendered PR-OCTA provides a novel approach for quantifying CNV complexity. Our results suggest that CNV acquiring more complex 3D vascular structure are associated with more frequent long-term anti-VEGF therapy, reflecting a particular pattern of normalization or complex CNV remodeling process that characterizes these less responsive eyes.

Keywords: choroidal neovascularization, OCT, optical coherence tomography angiography, AMD

Anti-VEGF is highly effective therapy for neovascular AMD (nAMD).[1–3] Although monthly intravitreal injections have generally been associated with the most favorable results in randomized controlled clinical trials, this strategy represents a significant treatment and financial burden.[4] Studies using individualized injection regimens, such as pro re nata and treat-and-extend, have shown comparable functional and anatomic results to monthly regimens, with the advantage of less frequent injections.[5] However, identifying the most effective individualized treatment algorithm for each patient with nAMD remains challenging, as clinicians largely rely on trial and error.[6,7]

With the introduction of optical coherence tomography angiography (OCTA), studies set out to explore whether choroidal neovascular (CNV) morphologic parameters can be used to predict treatment response.[8–15] These studies have yielded conflicting results regarding the ability to predict CNV activity (leakage) based on qualitative OCTA parameters, such as CNV shape, vessel caliber, termini morphology,[14,15] or quantitative parameters, such as vessel density, branching index, lacunarity, and fractal dimension.[8,13,16] The diverse outcomes of these studies could be related to the wide range of lesion characteristics, duration of CNV, number of previous anti-VEGF injections, or the length of interval between initiation of anti-VEGF therapy and OCTA imaging. The "normalization hypothesis" suggests that with continued anti-angiogenic therapy, newly formed, abnormally shaped vessels gradually acquire more "normal" vascular patterns as they become less tortuous, with improved endothelial barrier and decreased leakage as a result of pericyte coverage.[17] The dynamic nature of the microvasculature during therapy is therefore another potential variable influencing the diverse results in these previous OCTA studies.

OCTA studies have significantly enhanced our understanding of the microvascular characteristics of nAMD, but have not yet provided clear guidelines for clinicians on how to harness OCTA technology to enhance the management of the individual patient. Importantly, these studies were limited by the compression of the complex three-dimensional (3D) OCTA data into two-dimensional (2D) en face images. Furthermore,

most of these studies did not adequately address the projection artifact, where flow signals in more superficial blood vessels, including CNV, are projected onto the deeper layers of the OCTA volume, which may confound interpretations of CNV vasculature.[18]

The Submacular Surgery Trials, as well as work by Grossniklaus et al.,[13,19-21] provided an improved pathological understanding of the CNV in nAMD using surgical specimens and donor eyes. Donor eye studies showed that CNV membranes grow above Bruch's membrane in a plane parallel to, and mimicking the morphology and functional characteristics of, the choriocapillaris.[22-24] Unfortunately, these histological studies were performed before the introduction of anti-VEGF and may not entirely capture the current state of CNV pathology in the era of anti-VEGF. OCT studies have identified features of large vascularized pigment epithelial detachments (PEDs) that can grow to considerable height above Bruch's membrane.[25,26] These studies reported multilayered structural components within vascularized PEDs, a pattern that is distinct from the planar morphology suggested in histopathologic studies predating the introduction of anti-VEGF.[21]

In the current study, we hypothesized that CNVs that acquire a complex 3D microvascular structure could be associated with more active CNV leakage and hence require more frequent treatment during individualized therapy in nAMD. Therefore, we used projection-resolved (PR)-OCTA and 3D volume rendering to study the complexity of CNV lesions, as well as to explore the characteristics associated with their responsiveness to anti-VEGF agents and visual outcome.

METHODS

This was a retrospective analysis of patients undergoing individualized treatment for nAMD recruited in the Department of Ophthalmology at Northwestern University in Chicago, IL, USA, between August 2015 and October 2016. This study was approved by the Institutional Review Board of Northwestern University and followed the tenets of the Declaration of Helsinki. This study was performed in accordance with the Health Insurance Portability and Accountability Act regulations. Written informed consent was obtained from all study participants.

Study Sample

Inclusion criteria were a diagnosis of CNV secondary to AMD, equivalent to grade 4 on the Age-Related Eye Disease Study scale scale,[27] and sufficient time from initiation of anti-VEGF therapy to have reached a stable treatment schedule (minimum 6 months of follow-up during treatment). We included eyes with type 1 CNV (vascularized PED), type 2 CNV (subretinal), and type 4 CNV (polypoidal). Polypoidal choroidal vasculopathy was diagnosed based on the presence of a shallow PED on OCT with "double layer sign" confirmed as a branching vascular network on indocyanine green angiography (ICGA) along with a peaked PED on OCT confirmed as polyps on ICGA.[28,29] We included eyes treated with ranibizumab, bevacizumab, or aflibercept, or any combination of the three anti-VEGF agents. Only eyes that had OCTA images without movement or shadow artifacts in the area of interest were considered eligible for further analysis. All patients received a loading series of three injections followed by either a pro re nata or treat-and-extend regimen at the discretion of the treating physician. Treatment/follow-up intervals were generally extended increasingly by 2 weeks once patients achieved a dry retina.

Exclusion criteria were eyes with previous surgical retinal repair and those with other retinal disease such as high myopia (over −7 D) that may influence our results. We excluded eyes with type 3 CNV (retinal angiomatous proliferation) due to the retinal (as opposed to choroidal) origin of these lesions. We excluded patients with significant cataracts (above nuclear opalescence grade 3 or nuclear color grade 3).[30]

Electronic medical records were reviewed to obtain demographic and clinical information. Monocular visual acuity (VA) at the time of first OCTA imaging session was determined using Snellen eye charts under dim illumination and converted to logMAR as previously described.[31]

OCTA Imaging

We acquired 3×3 mm^2 OCTA scans centered on the fovea using the RTVue-XR Avanti system (Optovue, Inc., Fremont, CA, USA), which incorporates split-spectrum amplitude-decorrelation angiography (SSADA) software.[32] This device uses a light source centered on 840 nm with a full-width at half maximum bandwidth of 45 nm and an A-scan rate of 70,000 scans per second. At each location on the retina, the RTVue system captures two consecutive B-scans (M-B frames) each containing 304 A-scans. The final 3×3 mm^2 scan contains a total of 304 B-scans, each with 304 A-scans. An orthogonal registration algorithm was used to reduce motion artifacts and improve the signal-to-noise ratio.[33] The SSADA algorithm then extracts angiographic information by quantifying the decorrelation of the OCT reflectance between the two consecutive B-scans. Only images with signal strength index (SSI) above 50 were eligible for further analysis (manufacturer-recommended SSI cutoff value >39). Both automatic and manual segmentation methods were used for en face visualization of CNV, but because only cross-sectional quantitative parameters were used, variability in segmentation did not affect the results of this study.

Patient Classification

We classified eyes based on the individualized anti-VEGF treatment interval (frequency of injections) that achieved a "dry retina." "Good responders" were defined as needing treatment less frequently than every 6 weeks, whereas "poor responders" required treatment every 6 weeks or more frequently.[16] The classification of good versus poor response to anti-VEGF was determined based on average treatment interval for each patient from initiation of anti-VEGF therapy to time of analysis. A minimum of 6 months following initial therapy was a prerequisite for inclusion in this study, but there was no standardized interval from onset of therapy to first imaging session. For a subgroup analysis, we classified eyes based on the interval between the initiation of anti-VEGF therapy and OCTA imaging into short- and long-term imaging groups (imaging at less or more than 12 months, respectively).

PR-OCTA Post-Processing

We implemented a version of the PR-OCTA algorithm previously described by Zhang et al.[34] in a custom MATLAB (Mathworks 2015, Natick, MA, USA) program. This algorithm has been used to study the three macular capillary plexuses of the inner retina.[35] The authors reported that the OCTA projection tail artifacts have lower decorrelation values than real vessels. The algorithm removes projection artifacts by searching for and preserving consecutively increasing decorrelation peaks (real vessels) along each A-line. The OCTA values at the peak positions are kept, whereas the remaining pixels in the A-scan are set to zero, resulting in the removal of projection
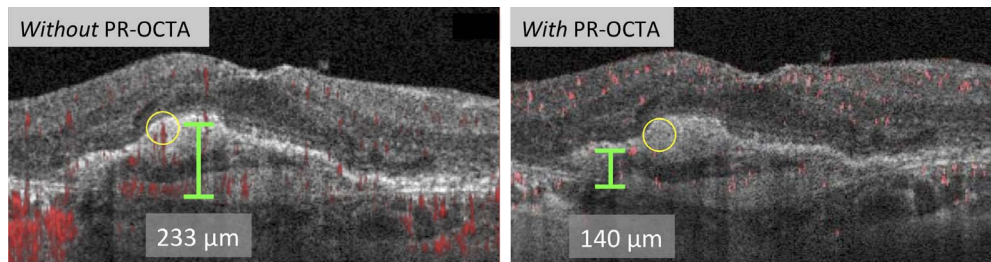
FIGURE 1. PR-OCTA improves quantitative analysis of CNV. *Left*: Cross-sectional OCTA without PR-OCTA showing highest CNV flow signal measurement. The *yellow circle* represents a projection artifact that could be incorrectly graded as highest CNV flow signal. *Right*: Cross-sectional OCTA with PR-OCTA showing elimination of projection artifacts (*yellow circle*), and hence more accurate CNV flow signal height measurement.

artifacts. Figure 1 shows an example in which PR-OCTA eliminated projection artifacts, allowing more accurate quantification of the true CNV flow signal height on cross-sectional OCTA.

Image Analysis

Two masked, independent graders (PLN and ADT) used cross-sectional PR-OCTA to evaluate two cross sections with the highest CNV flow signal. To standardize the approach, a senior grader identified and exported the two B-scans with the highest apparent CNV flow signal from within the entire imaging volume. Then, each masked grader independently assessed the same B-scan for highest CNV flow signal. "Highest CNV flow signal" was defined as the most anterior point of

CNV flow signal (decorrelation signal), or in other words, the CNV flow signal farthest from Bruch's membrane. Images were exported into ImageJ (http://imagej.nih.gov/ij/; provided in the public domain by the National Institutes of Health, Bethesda, MD, USA). The Line Tool was used to measure the distance between Bruch's membrane and the highest point of CNV flow signal. The greater of the two measurements for each grader was recorded for each eye.

Each PR-OCTA volume was then assessed for two additional parameters: the number of CNV flow layers and the CNV flow signal thickness (Fig. 2). "Number of CNV flow layers" was defined as the number of layers of pathological decorrelation signal that were separated by at least 30 μm in the axial direction (Fig. 3). CNV flow layers that were separated by less
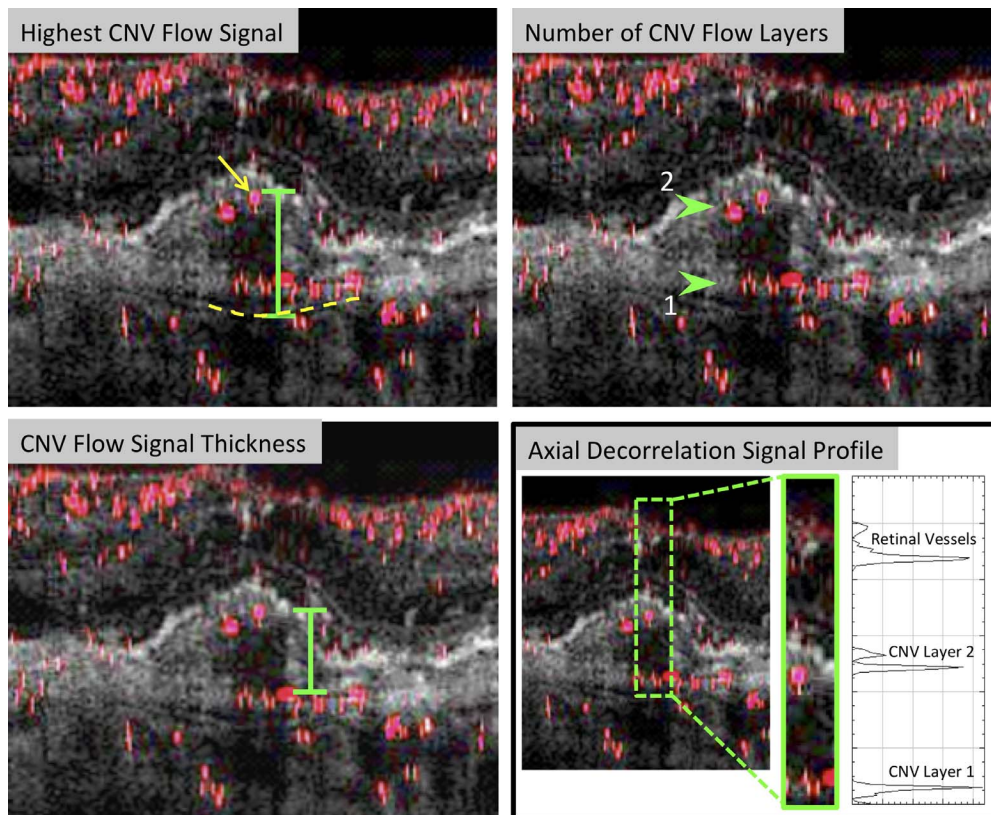

FIGURE 2. Quantitative parameters of CNV in PR-OCTA. "Poor responder" from short-term follow-up group. *Top left*: Cross-sectional PR-OCTA showing "Highest CNV Flow Signal" measurement, which is the distance between Bruch's membrane (*dotted yellow line*) and the most anterior CNV decorrelation signal (*yellow arrow*). *Top right*: Cross-sectional PR-OCTA with "Number of CNV Flow Layers" (*n* = 2; *green arrows*). *Bottom left*: Cross-sectional PR-OCTA showing "CNV Flow Signal Thickness" measurement, which is the distance between the most anterior and most posterior CNV flow layer (*green*). *Bottom right*: Axial plot profile of decorrelation signal intensity. From top to bottom, the three peaks are: (1) the inner retinal capillaries near the edge of the foveal avascular zone, (2) CNV flow layer 2, and (3) CNV flow layer 1.
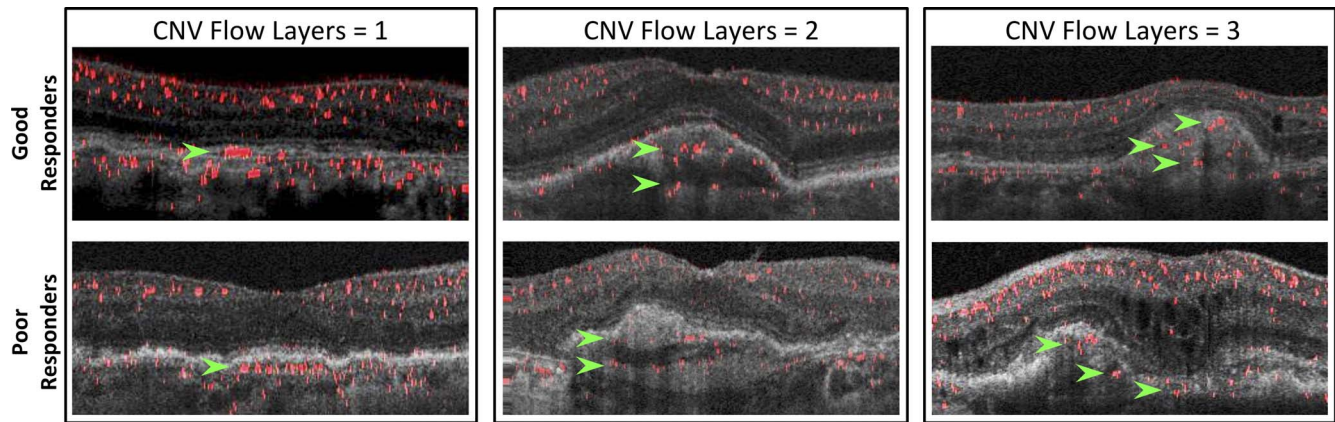
FIGURE 3. Examples of CNV membranes with increasing CNV flow layers. *Top row*: Good responder CNVs. *Bottom row*: Poor responder CNVs. The number of CNV flow layers increases from left to right (one to three layers). *Green arrows* point to each individual CNV flow layer.

than 30 μm were counted as a single CNV flow layer because the axial resolution of the device is 15 μm at best. To ensure that CNV flow layers were not projection artifact, we evaluated the intensity of the decorrelation signal using the Plot Profile tool in ImageJ (Fig. 2). In CNVs with more than one flow layer, we also measured the "CNV flow signal thickness," defined as the distance between the most distal CNV flow layers. For eyes with a single CNV flow layer, this value was recorded as zero. Highest CNV flow signal, number of CNV flow layers, and CNV flow signal thickness were averaged between the two graders and recorded for each eye. Figure 4 shows examples of the CNV flow signal appreciated within thick CNV lesions and CNV lesions underlying subretinal fluid or subretinal hyperreflective material.

Intraretinal hyperreflective foci have been identified as important precursors of nAMD progression.[36–39] We therefore evaluated the structural OCT volume for hyperreflective foci to assess whether their presence was associated with treatment response.

Three-Dimensional Volume Rendering

To perform 3D volume rendering of the PR-OCTA data, we loaded the retinal layer segmentation provided by the Angiovue software (Optovue, Inc.) along with the PR-OCTA volume into a customized MATLAB program. We used the segmentations to remove the inner retinal capillary networks as well as the choroid and choriocapillaris, preserving only the outer retinal space. This approach enhanced the visualization
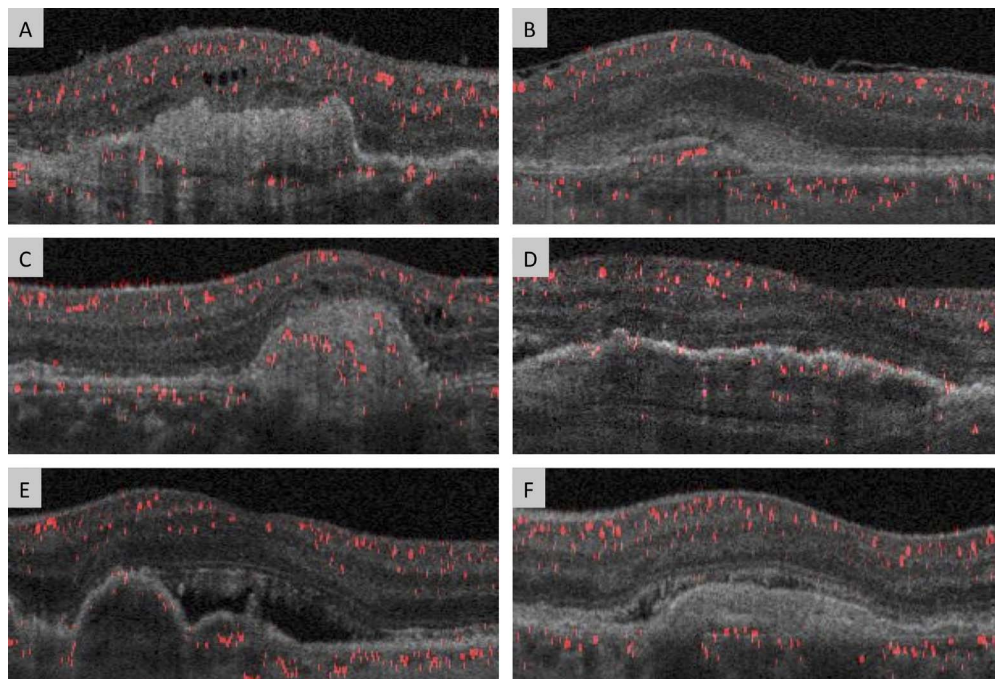

FIGURE 4. Examples of thick CNV membranes or CNV underlying subretinal fluid or hyperreflective material. (**A**) Poor responder with CNV flow signal is seen in the posterior side of thick CNV lesion. (**B**) Poor responder with CNV flow signal underlying subretinal hyperreflective material. (**D**) Good responder with CNV flow signals throughout thick lesion. (**C**) Good responder with CNV flow signal seen in multiple locations within the thick CNV lesion. (**D**) Poor responder with CNV flow signal seen in multiple locations within the thick CNV lesion. (**E**) Poor responder with CNV flow signal seen underlying an area of subretinal fluid. (**F**) Good responder with CNV flow signal seen on the posterior edge of a thick CNV lesion.

TABLE 1. Demographic Characteristics of Patients With Neovascular AMD

Responder Group	All Subjects			Short-Term Imaging Group, 0–12 mo			Long-Term Imaging Group, >12 mo		
	Good	Poor	*P*	Good	Poor	*P*	Good	Poor	*P*
Patients, *n* (eyes)	28 (29)	21 (22)	–	9 (9)	7 (7)	–	19 (20)	14 (15)	–
Age (SD)	75.4 (14.1)	76.9 (8.5)	0.67	74.6 (17.4)	75.9 (9.3)	0.86	75.7 (12.4)	77.5 (8.1)	0.63
Females, *n* (%)	12 (42.9)	14 (66.7)	0.10	2 (22.2)	7 (100.0)	<0.01*	10 (52.6)	7 (50.0)	0.89
LogMAR VA (SD)	0.37 (0.39)	0.36 (0.25)	0.90	0.42 (0.25)	0.42 (0.32)	0.98	0.35 (0.45)	0.33 (0.21)	0.89
Months from 1st injection to OCTA (SD)	30.2 (22.7)	33.1 (34.9)	0.72	6.1 (4.4)	2.4 (4.3)	0.12	41.1 (18.7)	47.4 (33.6)	0.48
Treatment interval in weeks (SD)	11.4 (6.8)	4.6 (1.2)	<0.01*	9.3 (2.3)	4.9 (0.7)	<0.01*	12.3 (7.9)	4.4 (1.3)	<0.01*
Previous injections, *n* (SD)	15.2 (12.2)	45.1 (37.7)	<0.01*	5.8 (3.5)	10.9 (6.1)	0.054	19.4 (12.4)	61.1 (35.4)	0.011*

The demographic characteristics comparing good and poor responders were largely balanced. The one exception was a greater proportion of females in the poor responder short-term group. Short-term group: patients who had OCTA imaging within 12 months of initial anti-VEGF treatment. Long-term group: patients who had OCTA imaging more than 12 months after their initial anti-VEGF treatment.

* Statistical significance ($P < 0.05$).

of CNV lesions and allowed us to rotate the lesion and examine different perspectives. Next we exported the outer retinal space with the CNV to a binary file. We loaded the binary file using the commercial visualization software Amira (Visualization Sciences Group, Bordeaux, France, and the Zuse Institute, Berlin, Germany). Volume-rendered images were exported as videos.

Statistics

We performed statistical tests with SPSS version 21 (IBM SPSS Statistics; IBM Corporation, Chicago, IL, USA). Independent samples *t* tests were used to compare PR-OCTA parameters, as well as demographic characteristics for the following groups: (1) all subjects: good versus poor responders, (2) short-term imaging: good versus poor responders; and (3) long-term imaging: good versus poor responders. Two-way random intraclass correlation coefficients (ICCs) were used to assess reliability for PR-OCTA parameters. Shapiro-Wilk test was significant, indicating the data deviated from normal distribution. Levene's test for equality of variances was not significant, indicating homoscedasticity. Therefore, we performed nonparametric Spearman rank correlations to explore the relationships between VA and linear CNV complexity parameters (CNV flow signal thickness and highest CNV flow signal). Because "number of CNV flow layers" is a categorical variable, we used Kruskal-Wallis H Test with post hoc Dunn test to compare continuous variables (highest CNV flow signal with PR and VA) based on the number of CNV flow layers. Because CNVs with a single flow layer have a CNV flow thickness of zero, we compared only the CNV flow thickness between CNV with two and three flow layers using an independent samples *t*-test. We also used independent samples *t* tests to compare the means of continuous variables (highest CNV flow signal with PR, CNV flow signal thickness, and VA) based on hyperreflective foci (present or absent). A *P* value of less than 0.05 was considered statistically significant.

RESULTS

A total of 51 eyes from 49 patients (age 76.0 ± 11.9 years; range, 55–98) with CNV were included in this study. Twenty-nine (57%) of the 51 eyes were "good responders" and 22 (43%) were "poor responders." Overall, the demographic characteristics comparing good and poor responders were matched (Table 1). Of the poor responder eyes, 19 had type 1 CNV, 1 had type 2 CNV, and 2 eyes had type 4 CNV. Of the good responder eyes, 16 had type 1 CNV, 7 had type 2 CNV, and 6 eyes had type 4 CNV. On quantitative analysis, poor responders had significantly greater distance between Bruch's membrane and highest CNV flow signal ($P < 0.01$), a greater number of CNV flow layers ($P = 0.022$), and greater CNV flow thickness ($P < 0.01$; Table 2). Interestingly, significantly more eyes in the poor responder group had intraretinal hyperreflective foci compared with good responders ($P < 0.01$; Table 2). PR-OCTA parameters showed good intergrader reliability, as all ICCs were greater than 0.75 (Table 3). The use of 3D volume-rendered PR-OCTA improved the visualization of the number of CNV flow layers and examples are presented in Supplementary Videos S1 to S3.

TABLE 2. PR-OCTA Parameters Based on Response to Anti-VEGF Therapy

Responder Group	All Subjects			Short-Term Imaging Group, 0–12 mo			Long-Term Imaging Group, >12 mo		
	Good	Poor	*P*	Good	Poor	*P*	Good	Poor	*P*
Highest CNV flow signal, µm (SD)	90 (80)	152 (68)	<0.01*	104 (64)	177 (65)	0.040*	84 (87)	140 (68)	0.048*
No. of CNV flow layers	1.76 (0.69)	2.21 (0.63)	0.022*	2.06 (0.73)	2.14 (0.69)	0.811	1.63 (0.65)	2.23 (0.62)	<0.01*
CNV flow signal thickness, µm (SD)	63 (72)	123 (47)	<0.01*	72 (62)	131 (63)	0.083	58 (76)	120 (38)	<0.01*
Eyes with hyperreflective foci (%)	9 (31)	16 (73)	<0.01*	5 (56)	4 (57)	0.953	4 (20)	12 (80)	<0.01*
SSI (SD)	56 (4)	55 (4)	0.403	54 (3)	55 (4)	0.542	57 (4)	55 (5)	0.231

The poor responders in the long-term group had greater highest CNV flow signal on PR-OCTA, more CNV flow layers, greater CNV flow signal thickness, and a greater proportion of eyes with hyperreflective foci. Short-term group: patients who had OCTA imaging within 12 months of initial anti-VEGF treatment. Long-term group: patients who had OCTA imaging more than 12 months after their initial anti-VEGF treatment.

* Statistical significance ($P < 0.05$).

TABLE 3. Intergrader Reliability of PR-OCTA Parameters

	Short-Term Imaging Group, 0–12 mo ICC (95% CI)	Long-Term Imaging Group, >12 mo ICC (95% CI)
Highest CNV flow signal, μm (SD)	0.83 (0.70–0.87)	0.86 (0.74–0.93)
No. of CNV flow layers	0.84 (0.73–0.88)	0.89 (0.79–0.94)
CNV flow signal thickness, μm (SD)	0.81 (0.66–0.86)	0.78 (0.55–0.92)

There were good ICCs between two masked graders for the PR-OCTA parameter measurements. CI, confidence interval.

There was a weak correlation between VA and CNV flow signal thickness ($r = 0.305$, $P = 0.029$). We found no statistically significant relationship between VA and highest CNV flow signal ($r = 0.144$, $P = 0.312$). VA was not significantly different between groups based on number of CNV flow layers ($P = 0.756$). Highest CNV flow signal was significantly different between groups based on number of CNV flow layers ($P < 0.01$), and post hoc pairwise comparison showed the highest CNV flow signal was significantly greater in CNVs with three flow layers versus one flow layer ($P < 0.01$) (Fig. 5). We found no significant difference in CNV flow signal thickness between CNVs with two versus three CNV flow layers ($P = 0.631$). Highest CNV flow signal, CNV flow signal thickness, and VA were not significantly different when comparing eyes with and without hyperreflective foci ($P = 0.685$, $P = 0.281$, and $P = 0.556$).

In the subgroup analysis, 16 eyes of 16 patients were classified as "short-term" OCTA imaging (12 months or less from the initiation of anti-VEGF injections). This group underwent OCTA imaging an average 4 months from the initiation of anti-VEGF treatment, including nine eyes (56%) imaged at 3 months or less and five treatment-naïve eyes (31%) at time of imaging. The demographic characteristics comparing poor and good responders in the short-term group were matched, except there was a significantly higher number of females in the poor responder group ($P < 0.01$; Table 1). Poor responders had significantly greater highest CNV flow signal compared with good responders ($P = 0.040$), but differences in all other parameters lost statistical significance in the short-term group (Table 2).

The remaining 35 eyes of 33 patients were classified as "long-term," as they underwent OCTA imaging more than 12 months after their first injection. The 35 eyes in the long-term imaging group had a mean interval of 44 months from initial anti-VEGF treatment to OCTA imaging. Demographic characteristics were matched (Table 1) and quantitative CNV analysis showed overall similar statistical results as seen in the overall study population (Table 2).

DISCUSSION

This study demonstrates that 3D volume-rendered PR-OCTA analysis of CNV is a novel, quantitative, and reliable method for exploring the relationship between CNV vascular structure and treatment response in nAMD. By reducing the projection artifacts from the retinal vasculature and overlying CNV flow layers, the PR-OCTA algorithm provided a more accurate assessment of vascular CNV morphology than OCTA alone. We found that the height of the vascular components of CNV lesions in both short- and long-term imaging groups, as well as the 3D complexity (number of CNV flow layers) in the overall group and the long-term group (OCTA images taken at least a year after initial treatment), were associated with the frequency of anti-VEGF during individualized therapy. These findings highlight the importance of exploring the 3D vascular structure of CNV in OCTA and its association with the exudative propensity of nAMD. Our results also suggest that 3D OCTA parameters may hold promise for predicting CNV activity, especially when chronically treated lesions undergo vascular "normalization" and maturation.

In a previous OCTA study, Coscas et al.[14] found a significant correlation between qualitative en face OCTA parameters (i.e., shape, anastomoses) and CNV activity (i.e., necessity for treatment) in eyes with nAMD. In a qualitative analysis of nAMD, Miere et al.[15] found no association between CNV activity and en face OCTA parameters studied (i.e., perilesional hypointense halo, flow voids within CNV lesion). Although these studies provided important qualitative information about the microvascular structure of CNV in relation to disease activity, quantitative parameters that may be amenable to automatic detection will be attractive for large-scale studies.

Quantitative parameters previously studied include significantly greater fractal dimension (a marker of 2D vascular complexity) and a greater rate of small vessels branching and peripheral arcades in actively leaking compared with quiescent CNVs.[13] Interestingly, these authors found significantly lower fractal dimension in the inner aspects of the lesion during treatment, which suggests vascular "normalization" in response to antiangiogenic agents. Conversely, a recent study by our group found no association between en face OCTA parameters (i.e., branching index, average vessel length) and CNV disease activity or length of individualized treatment interval in treated CNV.[16] These conflicting results may be due to the different lesion criteria (i.e., subretinal fibrosis, number of previous injections) or endpoint definitions (i.e., OCTA parameters, disease activity) used in these studies. Perhaps more importantly, these studies are limited by the 2D analysis using only en face OCTA images, as well as the lack of
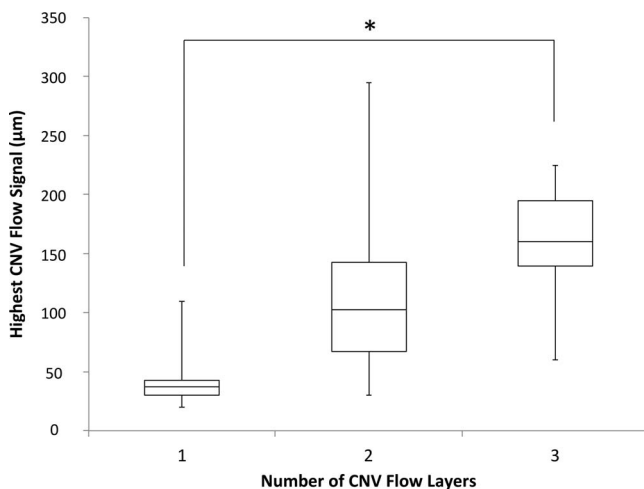
FIGURE 5. Box plot of highest CNV flow signal for CNV with different numbers of CNV flow layers. CNV with three flow layers had significantly greater highest CNV flow compared with CNV with one CNV flow layer (Kruskal-Wallis H Test with post hoc Dunn test, $P < 0.01$). *Asterisk* represents statistical significance.

correction for ubiquitous confounding variables in OCTA: projection artifacts.

Here, we explored the 3D complexity of CNV lesions with 3D volume rendering after removing projection artifacts using PR-OCTA. We classified eyes based on their treatment interval into good and poor responding eyes. We found that poor responders had a greater distance between Bruch's membrane and highest CNV flow signal, a greater number of CNV flow layers, and greater CNV flow signal thickness (Table 2). Comparing good and poor responder groups on OCTA images taken within a year of the initiation of anti-VEGF therapy (short-term imaging group, including treatment-naïve eyes), we found that poor responders had, on average, a greater distance from highest CNV flow signal to Bruch's membrane (Table 2). None of the other parameters were significantly different between good and poor responders in the short-term group. When we assessed the same parameters in eyes with OCTA images taken more than 1 year after initial anti-VEGF injection (long-term imaging group), the differences between groups became significant (Table 2). We found high ICC between the two masked graders, suggesting reliability for these measurements.

The findings in the long-term imaging group suggest that during "normalization" of the tortuous, leaky, highly branching CNV vessels and along with the acquisition of pericyte coverage during anti-VEGF therapy, the "poor responder" CNVs become more complex in 3D. We therefore hypothesize that there could be two modes of nAMD response during antiangiogenic therapy. Lesions that show flattening of the CNV structure into a planar morphology, effectively recapitulating the choroid and maintaining adequate support of the previously hypoxic outer retina and RPE are able to achieve effective normalization and require less frequent treatment over time. In contrast, CNVs that take on a multilayered, complex microvascular structure may represent a less effective form of normalization, where these CNV continue to grow, leak, and deposit fibrin, and hence require more frequent injections.

Pathologically, it is thought that fibrin, one of the most common extracellular components of CNV,[20,40–42] likely serves as a scaffold for CNV growth.[43] Histologically, fibrin has been found to cover the lateral edges of some CNVs, whereas in others it is seen covering the entire inner surface of the CNV core.[40] We postulate that the degree and location of fibrin deposition likely plays a role in the development of the complex CNV structure as well as the number of CNV flow layers, which in our study was associated with therapeutic response. Indeed, larger 2D CNV lesion size has been associated with greater loss of visual function,[44,45] as well as poorer response to anti-VEGF treatment.[46,47] In our study, 3D volume-rendered PR-OCTA (Supplementary Videos S1–S3) provides further evidence for the presence of vascularized, multilayered CNVs. Interestingly, we found the CNV height and number of flow layers showed significant differences only at extremes of CNV complexity, suggesting these variables may not be interchangeable, and that the thickness of intervening nonvascular tissue (potentially fibrin and fibrous elements) is highly variable (Fig. 5). The lack of significant differences in CNV complexity parameters (other than highest CNV flow signal) in the short-term group could also reflect acute pathological changes: debris (fibrin, hemorrhage, exudates) in the early stages of CNV that resolve quickly with treatment, whereas more stable fibrous scaffolds are likely to exist in mature CNVs interspersed between the vascular layers and Bruch's membrane.

OCT studies in eyes with non-neovascular AMD have identified hyperreflective foci as high-risk precursors associated with the risk of developing nAMD.[36–39] In this study, we found that poor responders overall, as well as in the long-term group, showed a significantly greater prevalence of hyperreflective foci compared with good responders. We did not find any significant relationships between hyperreflective foci and VA or any of the CNV complexity parameters. Further longitudinal studies with larger cohorts are needed to confirm whether the presence of hyperreflective foci during anti-VEGF therapy is associated with higher CNV activity and the need for more frequent therapy.

We found a significant correlation between VA and CNV flow signal thickness, but not between VA and any other CNV variable in our study. This may be due to variable location of the CNV, the presence or absence of fluid, and the extent of fibrosis, which were not evaluated in this study. We found that eyes with more CNV flow layers had greater highest CNV flow height measurements, and this was statistically significant when comparing CNVs with one flow layer with those with three flow layers (Fig. 5). This suggests that highest CNV flow signal (or CNV flow signal thickness) may not sufficiently capture the complexity of CNV on cross-sectional OCTA except perhaps at extremes of complexity. Future large-scale studies will be important to further characterize and study these novel CNV complexity parameters.

Limitations of this study include the limited number of eyes, as well as the cross-sectional nature and the limited number of treatment-naïve eyes. Future longitudinal studies using PR-OCTA parameters will be important to further elucidate the 3D evolution of CNV in response to therapy. Another limitation is the use of SD-OCTA, which suffers from sensitivity roll-off leading to signal attenuation at greater retinal depths. Future studies using swept-source OCTA may be important to validate our findings. Due to a limited sample size, different CNV types and anti-VEGF medications were not analyzed separately, which may be an important area for future studies. Indeed, good responders in our study population had a greater proportion of type 2 and type 4 CNV, but other study populations may reveal different patterns. Furthermore, our approach for quantifying CNV using cross-sectional PR-OCTA, while reliable with high intergrader ICC, is novel; hence, future validation studies will be important.

Conclusions

In conclusion, using 3D PR-OCTA we have identified novel CNV complexity parameters that are associated with CNV activity and treatment response in nAMD. Furthermore, we highlight the advantages of using PR-OCTA and 3D volume rendering for the accurate analysis and visualization of CNV, respectively. Automated algorithms for projection resolution and volume rendering of OCTA images may therefore prove useful in the future as we begin to unravel the importance and implications of 3D CNV complexity.

References

1. Rosenfeld PJ, Brown DM, Heier JS, et al. Ranibizumab for neovascular age-related macular degeneration. *N Engl J Med*. 2006;355:1419–1431.

2. Avery RL, Pieramici DJ, Rabena MD, Castellarin AA, Ma'an AN, Giust MJ. Intravitreal bevacizumab (Avastin) for neovascular

age-related macular degeneration. *Ophthalmology*. 2006;113: 363–372.e365.

3. Martin DF, Maguire MG, Ying GS, Grunwald JE, Fine SL, Jaffe GJ. Ranibizumab and bevacizumab for neovascular age-related macular degeneration. *N Engl J Med*. 2011;364:1897–1908.

4. Grunwald JE, Daniel E, Huang J, et al. Risk of geographic atrophy in the comparison of age-related macular degeneration treatments trials. *Ophthalmology*. 2014;121:150–161.

5. Schmidt-Erfurth U, Chong V, Loewenstein A, et al. Guidelines for the management of neovascular age-related macular degeneration by the european society of retina specialists (Euretina). *Br J Ophthalmol*. 2014;98:1144–1167.

6. Fung AE, Lalwani GA, Rosenfeld PJ, et al. An optical coherence tomography-guided, variable dosing regimen with intravitreal ranibizumab (lucentis) for neovascular age-related macular degeneration. *Am J Ophthalmol*. 2007;143:566–583.e2.

7. Martin DF, Maguire MG, Fine SL, et al. Ranibizumab and bevacizumab for treatment of neovascular age-related macular degeneration: two-year results. *Ophthalmology*. 2012;119: 1388–1398.

8. Huang D, Jia Y, Rispoli M, Tan O, Lumbroso B. Optical coherence tomography angiography of time course of choroidal neovascularization in response to anti-angiogenic treatment. *Retina*. 2015;35:2260–2264.

9. Lumbroso B, Rispoli M, Savastano MC. Longitudinal optical coherence tomography–angiography study of type 2 naive choroidal neovascularization early response after treatment. *Retina*. 2015;35:2242–2251.

10. Jia Y, Bailey ST, Wilson DJ, et al. Quantitative optical coherence tomography angiography of choroidal neovascularization in age-related macular degeneration. *Ophthalmology*. 2014;121:1435–1444.

11. El Ameen A, Cohen SY, Semoun O, et al. Type 2 neovascularization secondary to age-related macular degeneration imaged by optical coherence tomography angiography. *Retina*. 2015;35:2212–2218.

12. Carnevali A, Cicinelli MV, Capuano V, et al. Optical Coherence Tomography angiography: a useful tool for diagnosis of treatment-naïve quiescent choroidal neovascularization. *Am J Ophthalmol*. 2016;169:189–198.

13. Al-Sheikh M, Iafe NA, Phasukkijwatana N, Sadda SR, Sarraf D. Biomarkers of neovascular activity in age-related macular degeneration using OCT angiography. *Retina*. 2018;38:220–230.

14. Coscas GJ, Lupidi M, Coscas F, Cagini C, Souied EH. Optical coherence tomography angiography versus traditional multimodal imaging in assessing the activity of exudative age-related macular degeneration: a new diagnostic challenge. *Retina*. 2015;35:2219–2228.

15. Miere A, Semoun O, Cohen SY, et al. Optical coherence tomography angiography features of subretinal fibrosis in age-related macular degeneration. *Retina*. 2015;35:2275–2284.

16. Roberts PK, Nesper PL, Gill MK, Fawzi AA. Semiautomated quantitative approach to characterize treatment response in neovascular age-related macular degeneration: a real-world study. *Retina*. 2017;37:1492–1498.

17. Jain RK. Normalization of tumor vasculature: an emerging concept in antiangiogenic therapy. *Science*. 2005;307:58–62.

18. Nesper PL, Lutty GA, Fawzi AA. Residual choroidal vessels in atrophy can masquerade as choroidal neovascularization on optical coherence tomography angiography: introducing a clinical and software approach [published online ahead of print October 20, 2017]. *Retina*. doi:10.1097/IAE.0000000000001863.

19. Grossniklaus HE, Green WR. Histopathologic and ultrastructural findings of surgically excised choroidal neovascularization. *Arch Ophthalmol*. 1998;116:745–749.

20. Grossniklaus H, Gass JD. Clinicopathologic correlations of surgically excised type 1 and type 2 submacular choroidal neovascular membranes. *Am J Ophthalmol*. 1998;126:59–69.

21. Grossniklaus HE, Green WR. Choroidal neovascularization. *Am J Ophthalmol*. 2004;137:496–503.

22. Kvanta A, Algvere P, Berglin L, Seregard S. Subfoveal fibrovascular membranes in age-related macular degeneration express vascular endothelial growth factor. *Invest Ophthalmol Vis Sci*. 1996;37:1929–1934.

23. Lopez PF, Sippy BD, Lambert HM, Thach AB, Hinton DR. Transdifferentiated retinal pigment epithelial cells are immunoreactive for vascular endothelial growth factor in surgically excised age-related macular degeneration-related choroidal neovascular membranes. *Invest Ophthalmol Vis Sci*. 1996;37: 855–868.

24. Green WR. Histopathology of age-related macular degeneration. *Mol Vis*. 1999;5:1–10.

25. Veronese C, Maiolo C, Morara M, Armstrong GW, Ciardella AP. Optical coherence tomography angiography to assess pigment epithelial detachment. *Retina*. 2016;36:645–650.

26. Rahimy E, Freund KB, Larsen M, et al. Multilayered pigment epithelial detachment in neovascular age-related macular degeneration. *Retina*. 2014;34:1289–1295.

27. Age-Related Eye Disease Study Research Group. The Age-Related Eye Disease Study system for classifying age-related macular degeneration from stereoscopic color fundus photographs: the Age-Related Eye Disease Study Report Number 6. *Am J Ophthalmol*. 2001;132:668–681.

28. Koh A, Lee WK, Chen L-J, et al. Everest Study: efficacy and safety of verteporfin photodynamic therapy in combination with ranibizumab or alone versus ranibizumab monotherapy in patients with symptomatic macular polypoidal choroidal vasculopathy. *Retina*. 2012;32:1453–1464.

29. Honda S, Matsumiya W, Negi A. Polypoidal choroidal vasculopathy: clinical features and genetic predisposition. *Ophthalmologica*. 2014;231:59–74.

30. Chylack LT, Wolfe JK, Singer DM, et al. The Lens Opacities Classification System III. *Arch Ophthalmol*. 1993;111:831–836.

31. Holladay JT. Proper method for calculating average visual acuity. *J Refract Surg*. 1997;13:388–391.

32. Jia Y, Tan O, Tokayer J, et al. Split-spectrum amplitude-decorrelation angiography with optical coherence tomography. *Opt Express*. 2012;20:4710–4725.

33. Kraus MF, Liu JJ, Schottenhamml J, et al. Quantitative 3D-OCT motion correction with tilt and illumination correction, robust similarity measure and regularization. *Biomed Opt Express*. 2014;5:2591–2613.

34. Zhang M, Hwang TS, Campbell JP, et al. Projection-resolved optical coherence tomographic angiography. *Biomed Opt Express*. 2016;7:816–828.

35. Hwang TS, Zhang M, Bhavsar K, et al. Visualization of 3 distinct retinal plexuses by projection-resolved optical coherence tomography angiography in diabetic retinopathy. *JAMA Ophthalmol*. 2016;134:1411–1419.

36. Christenbury JG, Folgar FA, O'Connell RV, et al. Progression of intermediate age-related macular degeneration with proliferation and inner retinal migration of hyperreflective foci. *Ophthalmology*. 2013;120:1038–1045.

37. Ouyang Y, Heussen FM, Hariri A, Keane PA, Sadda SR. Optical coherence tomography–based observation of the natural history of drusenoid lesion in eyes with dry age-related macular degeneration. *Ophthalmology*. 2013;120:2656–2665.

38. Zanzottera EC, Messinger JD, Ach T, Smith RT, Freund KB, Curcio CA. The Project Macula Retinal Pigment Epithelium Grading System for histology and optical coherence tomography in age-related macular degenerationrpe histology and

SDOCT correlates in AMD. *Invest Ophthalmol Vis Sci*. 2015; 56:3253–3268.

39. Roberts PK, Baumann B, Schlanitz FG, et al. Retinal pigment epithelial features indicative of neovascular progression in age-related macular degeneration. *Br J Ophthalmol*. 2017; 101:1361–1366.

40. Lafaut B, Bartz-Schmidt K, Broecke CV, Aisenbrey S, De Laey J, Heimann K. Clinicopathological correlation in exudative age related macular degeneration: histological differentiation between classic and occult choroidal neovascularisation. *Br J Ophthalmol*. 2000;84:239–243.

41. Spraul CW, Lang GE, Grossniklaus HE, Lang GK. Histologic and morphometric analysis of the choroid, Bruch's membrane, and retinal pigment epithelium in postmortem eyes with age-related macular degeneration and histologic examination of surgically excised choroidal neovascular membranes. *Surv Ophthalmol*. 1999;44:S10–S32.

42. Submacular Surgery Trials Research Group. Histopathologic and ultrastructural features of surgically excised subfoveal choroidal neovascular lesions. *Arch Ophthalmol*. 2005;123: 914–921.

43. Grossniklaus HE, Ling JX, Wallace TM, et al. Macrophage and retinal pigment epithelium expression of angiogenic cytokines in choroidal neovascularization. *Mol Vis*. 2002;8:119–126.

44. Boyer DS, Antoszyk AN, Awh CC, et al. Subgroup analysis of the MARINA Study of ranibizumab in neovascular age-related macular degeneration. *Ophthalmology*. 2007;114:246–252.

45. Rosenfeld PJ, Shapiro H, Tuomi L, Webster M, Elledge J, Blodi B. Characteristics of patients losing vision after 2 years of monthly dosing in the Phase III Ranibizumab Clinical Trials. *Ophthalmology*. 2011;118:523–530.

46. Lux A, Llacer H, Heussen FM, Joussen AM. Non-responders to bevacizumab (Avastin) therapy of choroidal neovascular lesions. *Br J Ophthalmol*. 2007;91:1318–1322.

47. Korb C, Zwiener I, Lorenz K, Mirshahi A, Pfeiffer N, Stoffelns B. Risk factors of a reduced response to ranibizumab treatment for neovascular age-related macular degeneration–evaluation in a clinical setting. *BMC Ophthalmol*. 2013;13:84.

SUPPLEMENTARY MATERIAL

SUPPLEMENTARY VIDEO S1. Volume-rendered PR-OCTA of CNV with three distinct flow layers. Right eye of 76-year-old female with type 1 (sub-RPE) CNV and a 19-month history of a total of 15 anti-VEGF injections with an average treatment interval of 5 weeks (poor responder). **(A)** En face OCTA of CNV without PR. **(B)** En face PR-OCTA of CNV. *Yellow line* indicates location of PR-OCTA B-scan **(C)**. **(C)** PR-OCTA B-scan with red flow overlay and segmentation boundaries for **(D)**. **(D)** Volume-rendered PR-OCTA video of CNV. The video begins with a cross-sectional view with the CNV oriented in the same direction as the en face images in **(A)** and **(B)**. Notice the triple-layered structure of the CNV membrane. From 11 to 16 seconds the *arrows* point to the connection of the CNV feeder vessel to the choroid.

SUPPLEMENTARY VIDEO S2. Volume-rendered PR-OCTA of CNV with two distinct flow layers. Right eye of 90-year-old female with mixed type 1 and 2 (sub-RPE and subretinal) CNV and a 13-month history of only two anti-VEGF injections with an average treatment interval of 26 weeks (good responder). **(A)** En face OCTA of CNV without PR. **(B)** En face PR-OCTA of CNV. *Yellow line* indicates location of PR-OCTA B-scan **(C)**. **(C)** PR-OCTA B-scan with red flow overlay and segmentation boundaries for **(D)**. **(D)** Volume-rendered PR-OCTA video of CNV. The video begins with a cross-sectional view of the CNV oriented the same as the B-scan in **(C)**. From 2 to 6 seconds the *arrows* point the second CNV flow layer.

SUPPLEMENTARY VIDEO S3. Volume-rendered PR-OCTA of CNV with single flow layer. Right eye of 88-year-old female with type 1 (sub-RPE) CNV and a 6-month history of five anti-VEGF injections with an average treatment interval of 5.6 weeks (poor responder). **(A)** En face OCTA of CNV without PR. **(B)** En face PR-OCTA of CNV. *Yellow line* indicates location of PR-OCTA B-scan **(C)**. **(C)** PR-OCTA B-scan with red flow overlay and segmentation boundaries for **(D)**. **(D)** Volume-rendered PR-OCTA video of CNV. The video begins with a cross-sectional view where the CNV orientation is the same as the B-scan in **(C)**.